Open Peer Review on Qeios

RESEARCH ARTICLE

Design, Synthesis, and In-Silico Analysis of Thiazole-Embedded Schiff Base Derivatives for Breast Cancer Therapeutic Potential

Maher Afroj Khanam[1], Ranajit Kumar Sutradhar[1], Ashutosh Nath[2], Mamiya Chowdhury[3], Keya Rani Dutta[1], Sanjay Belowar[4]

1 Chittagong University of Engineering and Technology, Bangladesh
2 University of Massachusetts Boston, Boston, United States
3 Dhaka University of Engineering and Technology, Bangladesh
4 BGMEA University of Fashion and Technology, Dhaka, Bangladesh

Funding: No specific funding was received for this work.

Potential competing interests: No potential competing interests to declare.

Abstract

Thiazole-derived Schiff base compounds possess significant pharmacological properties, influencing various enzymes in metabolic pathways and exhibiting antibacterial, antifungal, anti-inflammatory, antioxidant, and antiproliferative activities. This study delves into the synthesis, characterization, and in-silico analysis of ten thiazole-embedded Schiff base derivatives (TZ1-10), benchmarking them against five Food and Drug Administration (FDA)-approved breast cancer drugs. Molecular docking against multiple therapeutic targets related to fatty acid synthase and cell proliferation (PDB IDs: 4FX3, 4OAR, 3NUP, and 3ERT) alongside ADME and Lipinski rule assessments were conducted. Compounds TZ6 and TZ8 emerged as promising candidates with docking scores of -8.0 kcal/mol and -8.2 kcal/mol respectively against the 4FX3 protein. These findings contribute to a deeper understanding of thiazole-embedded Schiff base derivatives, showcasing their potential for future medicinal and scientific applications.

1. Introduction

In the realm of medicinal chemistry, Schiff bases have emerged as a versatile class of compounds exhibiting significant pharmacological potential[1]. These compounds, synthesized through the condensation of primary amines with carbonyl compounds, showcase diverse chemical structures that underlie their multifaceted medicinal properties[2]. Schiff bases have garnered attention for their therapeutic effects, including anti-inflammatory, analgesic, antibacterial, anticancer, and antioxidant activities[3]. Notably, their exceptional antioxidant properties are crucial for scavenging free radicals and alleviating oxidative stress, offering promise in addressing various pathological conditions, particularly metal-ion-related disorders[4]. The integration of computational studies into this field enhances our understanding of the structure-activity relationships that govern the medicinal potential of Schiff bases, facilitating rational drug design and illuminating their interactions with biological targets[5].

Thiazole, characterized by a five-membered ring containing four carbon atoms, one nitrogen atom, and one sulfur atom, exemplifies aromaticity and heteroatom diversity[6]. Thiazole rings serve as essential components in the design of molecules with varied functionalities, influencing electronic properties, lipophilicity, and molecular architecture. Consequently, these rings are valuable in medicinal chemistry, contributing to the development of pharmacologically active agents and enhancing the characteristics of polymers and materials in material science[7].

Breast cancer, which develops in breast cells, represents a significant health concern[8]. In 2018, breast cancer accounted for 25.4% of all cancer cases, making it the most prevalent type among women[9]. Current treatment modalities—including surgery, chemotherapy, hormone therapy, targeted therapy, and immunotherapy—are critical, with adjuvant chemotherapy being the primary approach in regions like China, where 81.4% of invasive breast cancer patients initiate chemotherapy[10]. However, recurrent clinical challenges such as medication resistance, disease recurrence, metastasis, and adverse drug reactions (e.g., diarrhea and emesis) underscore the pressing need for novel, cost-effective therapies with low toxicity to improve patient outcomes[11].

In this study, we focus on the characterization of thiazole-embedded Schiff base derivatives through spectroscopic techniques. Following this, we conducted in-silico computational analyses to evaluate the chemical stability and reactivity of the synthesized compounds. Moreover, molecular docking studies were performed to assess the inhibitory effects of these derivatives on breast cancer cells. Our findings aim to not only deepen the understanding of Schiff bases in therapeutic contexts but also to pave the way for the development of innovative treatments that address the limitations of current breast cancer therapies.

2. Materials and Methods

2.1. Materials

All starting materials and solvents were sourced from Sigma Aldrich and used without further purification. Uncorrected melting points were recorded using an Electrothermal melting point apparatus (model MPH-H290-264). Infrared spectra were measured by KBr disk on the SHIMADZU FTIR spectrophotometer (Model FTIR-IR Affinity-1) at Wazed Miah Scientific Research Centre, Jahangirnagar University, Savar, Dhaka. NMR spectra were obtained using a BRUKER AVANCE III HD (400 MHz) instrument, with chemical shifts recorded in δ units and referenced to the residual protons of the deuterated NMR solvent (1H). All spectral analyses were conducted at Wazed Miah Science Research Centre, Jahangirnagar University, Bangladesh.

2.2. Methods

2.2.1. *General Procedure for the Preparation of Thiosemicarbazone Derivatives (4-6)*

The synthesis of substituted thiosemicarbazone derivatives was conducted according to the method described by Al-

Amiery[12]. The reaction took place in an acidic medium, combining 0.01 mol of 4-substituted benzaldehyde (1) and 0.01 mol of thiosemicarbazide (2) in 20 mL of ethanol. This mixture was refluxed at 60 °C for 3 hours. After cooling to room temperature, the resulting-colored precipitate was filtered, washed with sodium bicarbonate solution, and recrystallized from 70% ethanol.

2.2.2. *Synthesis of Thiazole-Embedded Schiff Base Derivatives (TZ1-TZ3)*

A mixture of 0.013 mol of 3-chloroacetic acetone (3) and 0.015 mol of thiosemicarbazone derivatives (4-6) was dissolved in acetone and reflux 6 h. After completing reaction crude mixrue cooled in an ice bath. The cooled mixture was then added to ice-cold water to induce precipitation. The precipitate was filtered and recrystallized from ethanol, with compounds TZ1-TZ3 subsequently purified via column chromatography. Reaction shown in *Scheme 1*. All the reactions proceeded smoothly with diverse substituted thiosemicarbazone, and products were obtained in moderate yields. The structures of the synthesized compounds were elucidated by ^{1}H NMR, ^{13}C NMR, DEPT, HMBC spectroscopic method.

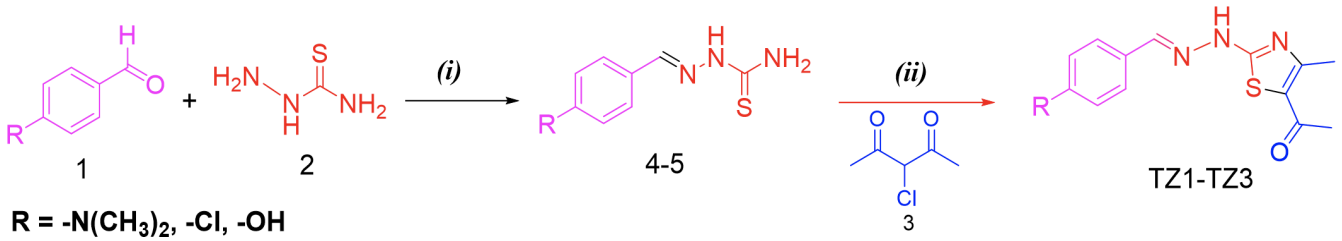

Scheme 1. Synthesis of thiosemicarbazone scaffold and thiazole-embedded Schiff base derivatives. The reaction conditions are as follows: (i) Catalytic amount of HCl in EtOH, reflux for 3 h at 60-70^{o}C, (ii) 3-chloroacetyl acetone in acetone, reflux for 6 h.

Physical properties of 2-(4-(dimethylamino) benzylidene) hydrazine-1-carbothioamide, 4:Orange colored powder, Yield 90%, m. p. 210~212 °C, IR (KBr, cm^{-1}, ***5***): 3406,3251(w, NH_2), 3051(C-H, Ar), 1593.99(C=N), 1184.29 (C=S), 815.85 (C-S-C). ^{1}HNMR (400 MHz, DMSO-d_6, δ ppm, ***5***): 7.59 (1H, d, J= 8.8 Hz, H-2′); 6.71 (1H, d, J= 8.4 Hz, H-3′);6.71 (1H, d, J= 8.4 Hz, H-5′) and 7.59 (1 H, d, J= 8.8 Hz, H-6′); 7.98 (1H, s, CH=N);3.36 (1H, s);11.04 (2H, s); 2.95 (2H, s). ^{13}C NMR (400 MHz, DMSO-d_6, δ ppm, ***5***): 121.8(C1'), 129.0(C2'), 112.1(C3'), 151.8(C4'), 112.1(C5'), 129.0(C6'), 143.8 (CH=N), 177.4(C=S),40.2N $(CH_3)_2$.

Physical properties of 2-(4-chlorobenzylidene) hydrazine-1-carbothioamide, 5:Brown coloured crystal, Yield 93%, m. p. 222~225 °C, IR (KBr, cm^{-1}, ***6***): 3468,3360(w, NH_2), 1587.47(C=N), 1234.44 (C=S), 877.46 (C-S-C). ^{1}HNMR (400 MHz, DMSO-d_6, δ ppm, ***6***): 7.59 (1H, d, J= 8.8 Hz, H-2′); 6.71 (1H, d, J= 8.4 Hz, H-3′);6.71 (1H, d, J= 8.4 Hz, H-5′) and 7.59 (1 H, d, J= 8.8 Hz, H-6′); 7.98 (1H, s, CH=N);3.36 (3H, s);2.95(2H, s). ^{13}C NMR (400 MHz, DMSO-d_6, δ ppm, ***6***): 125.5(C1'), 129.9(C2'), 116.0(C3'), 159.7(C4'), 116.0(C5'), 129.5 (C6'),143.2(CH=N), 177.8(C=S).

Physical properties of (E)-2-(4-hydroxybenzylidene) hydrazine-1-carbothioamide, 6:White powder, Yield 75%, m. p. 213 ~ 215 °C, IR (KBr, cm^{-1}, ***7***): 3560,3150.40(NH_2), 1612.40 (C=N), 1275.02 (C=S), 844.82 (C-S-C). ^{1}HNMR (400 MHz, DMSO-d_6, δ ppm, ***7***): 7.59 (1H, d, J= 8.8 Hz, H-2′); 6.71 (1H, d, J= 8.4 Hz, H-3′);6.71 (1H, d, J= 8.4 Hz, H-5′) and 7.59 (1

H, d, J= 8.8 Hz, H-6′); 7.98 (1H, s, CH=N);3.36 (3H, s);2.95(2H, s). ^{13}C NMR (400 MHz, DMSO-d_6, δ ppm, ***7***): 133.0(C1'), 129.4(C2'), 129.1(C3'), 134.7(C4'), 129.1(C5'), 129.4 (C6), 141.0(CH=N), 178.5(C=S).

Physical properties of 1-(2-(2-(4-(dimethylamino) benzylidene) hydrazineyl)-4-methylthiazol-5-yl) ethan-1-one, TZ1: Brown powder, Yield 55%, m.p.228~230 °C, IR (KBr, cm^{-1}, ***TZ1***): 3160 (NH), 3070 (w, C-H, Ar), 1604.77 (C=O), 1525.60 (C=N),1300.67, 1178.51 (C=S). ^{1}HNMR (400 MHz, DMSO-d_6, δ ppm, ***TZ1***: 7.50 (1H, d, J= 8.4 Hz, H-2′); 6.75 (1H, d, J= 8.4 Hz, H-3′);6.75 (1H, d, J= 8.4 Hz, H-5′); 7.50 (1H, d, J= 8.4 Hz, H-6′); 7.98 (1H, s, CH=N);3.38 (s);2.95(s). ^{13}C NMR (400 MHz, DMSO-d_6, δ ppm, ***TZ1***): 121.7(C1'), 129.0(C2'), 112.1(C3'), 151.9(C4'), 112.3(C5'), 129.0(C6'), 146.3(CH=N), 169.3(C=S), 111.5(C2"), 128.5(C4"), 189.0(C=O), 29.9(COCH$_3$), 18.7(4"-CH$_3$), 40.2N(CH$_3$)$_2$.

Physical properties of 1-(2-(2-(4-chlorobenzylidene) hydrazineyl)-4-methylthiazol-5-yl) ethan-1-one, TZ2: Light brown colored crystal, Yield 55%, m.p.190~192°C, IR (KBr, cm^{-1}, ***TZ2***): 3560, 3150 (NH), 3014.74, 2926 (w, C-H, Ar), 1612.40 (C=O), 1512.19 (C=N),1275.02 (C=S).^{1}HNMR (400 MHz, DMSO-d_6, δ ppm, ***TZ2***): 2.51(s, 3H, CO-CH$_3$), 2.41(s, 3H, H-4′), 7.55 (d,1H, H-2', J = 8.4 Hz), 6.86 (d, 1H, H-3′, J = 8.4 Hz), 6.86 (d,1H, H-5′, J = 8.4 Hz) and 7.55 (d,1H, H-5′, J = 8.4 Hz), 8.11 (s, 1H, CH=N). ^{13}C NMR (400 MHz, DMSO-d_6, δ ppm, ***TZ2***): 125.1(C1'), 129.2(C2'), 116.2(C3'), 160.1(C4'), 116.2(C5'), 129.2(C6'), 147.0(CH=N), 168.8(C=S), 122.0(C2"), 154.6(C4"), 189.3(C=O), 29.9(COCH$_3$), 17.9(4"-CH$_3$).

Physical properties of 1-(2-(2-(4-hydroxybenzylidene) hydrazineyl)-4-methylthiazol-5-yl) ethan-1-one, TZ3: White colored powder, Yield 55%, m.p. 242~244°C, IR (KBr, cm^{-1}, ***TZ3***): 3414 (w, OH Ar),2738, 2645 (NH), 1622 (C=O), 1494 (C=N), 1240 (C=S). ^{1}HNMR (400 MHz, DMSO-d_6, δ ppm, ***TZ3***): 2.41(s, 3H, H-4′), 2.51(s, 3H, CO-CH$_3$), 5.38 (s,1H, NH), 7.72 (d,1H, H-2′, J = 8.0Hz), 7.51(d, 1H, H-3′, J = 8.4Hz), 7.51 (d,1H, H-5′, J = 8.4Hz), 7.72 (d,1H, H-6′, J = 8.0Hz), 8.16 (s,1H, HO-4′ and CH=N). ^{13}C NMR (DMSO-d_6, 400 MHz) δ: 133.0(C1'), 129.4(C2'), 129.1(C3'), 134.7(C4'), 129.1(C5'), 129.4 (C6), 141.0(CH=N), 178.5(C=S).

2.2.3. *Computational methods*

1. DFT Calculation

The structural properties of thiazole derivatives were modified and optimized using Gaussian 09[13] W Revision D.01. Visualization was carried out using Gauss View 6.0.16[13] software. Density Functional Theory (DFT) with the B3LYP functional and 6-311++G (d, p) basis set was applied to calculate spectral and physicochemical properties in the gas phase. Vibrational frequencies were confirmed to match minima on the potential energy surface, and molecular orbital characteristics were analyzed to assess chemical reactivity. [14]

2. Thiazole Derivatives (TZ) Optimization, Protein Preparation, and Molecular Docking

Gauss View 6.0.16 was utilized to prepare the Gaussian input files (.gif) for Thiazole derivatives (TZ1-10). Each structure was optimized using Gaussian 09 and the B3LYP method. Protein structures were obtained from the RCSB Protein Data Bank (PDB). The specific proteins used were Homo sapiens *Spodoptera frugiperda* (PDB ID: 4FX3),[15] Homo sapiens

Peptide from Nuclear receptor corepressor 2 (protein), Progesterone receptor (protein) (4OAR), [16] Homo sapiens Cell division protein kinase 6 (protein) (3NUP), [17] and Homo sapiens *Escherichia coli* (3ERT). [18] Prior to docking, water molecules were removed, and original ligands were extracted. Ligands were docked against proteins using Autodock Vina [19] on the PyRx [20] workstation, with the grid box positioned around the macromolecule's active site. Visualization of receptor-ligand binding interactions was performed using Biovia Discovery Studio [21] 2024 Client.

3. Analysis of Drug Likeness of TZ1-10

Toxicity and pharmacokinetic properties were assessed using the updated AdmetSAR version 2.0 [21] (http://lmmd.ecust.edu.cn/admetSAR2/). Drug-like properties of the compounds TZ (1-10) were analyzed using the Molinspiration online server [22] (https://www.molinspiration.com/cgi-bin/properties).

3. Result and Discussion

3.1. Chemistry

Scheme 1 illustrates the reaction between 3-chloroacetylacetone and thiosemicarbazones, resulting in the formation of thiazole-embedded Schiff base derivatives (TZ1-TZ3). Structural diversity is achieved by varying substitutions on the thiosemicarbazone scaffold (Figure X). The synthesized compounds were characterized by ^{1}H NMR, ^{13}C NMR, and IR spectroscopy. IR spectra confirmed the presence of key functional groups, including NH, C=S, C=O, and C=N. In the ^{1}H NMR spectra, distinct chemical shifts corresponding to protons on the thiazole and Schiff base moieties were observed. The ^{13}C NMR spectra showed characteristic signals for carbonyl, thiazole, and Schiff base carbons. All the spectral data of synthesized compounds are given in Table 1-3.

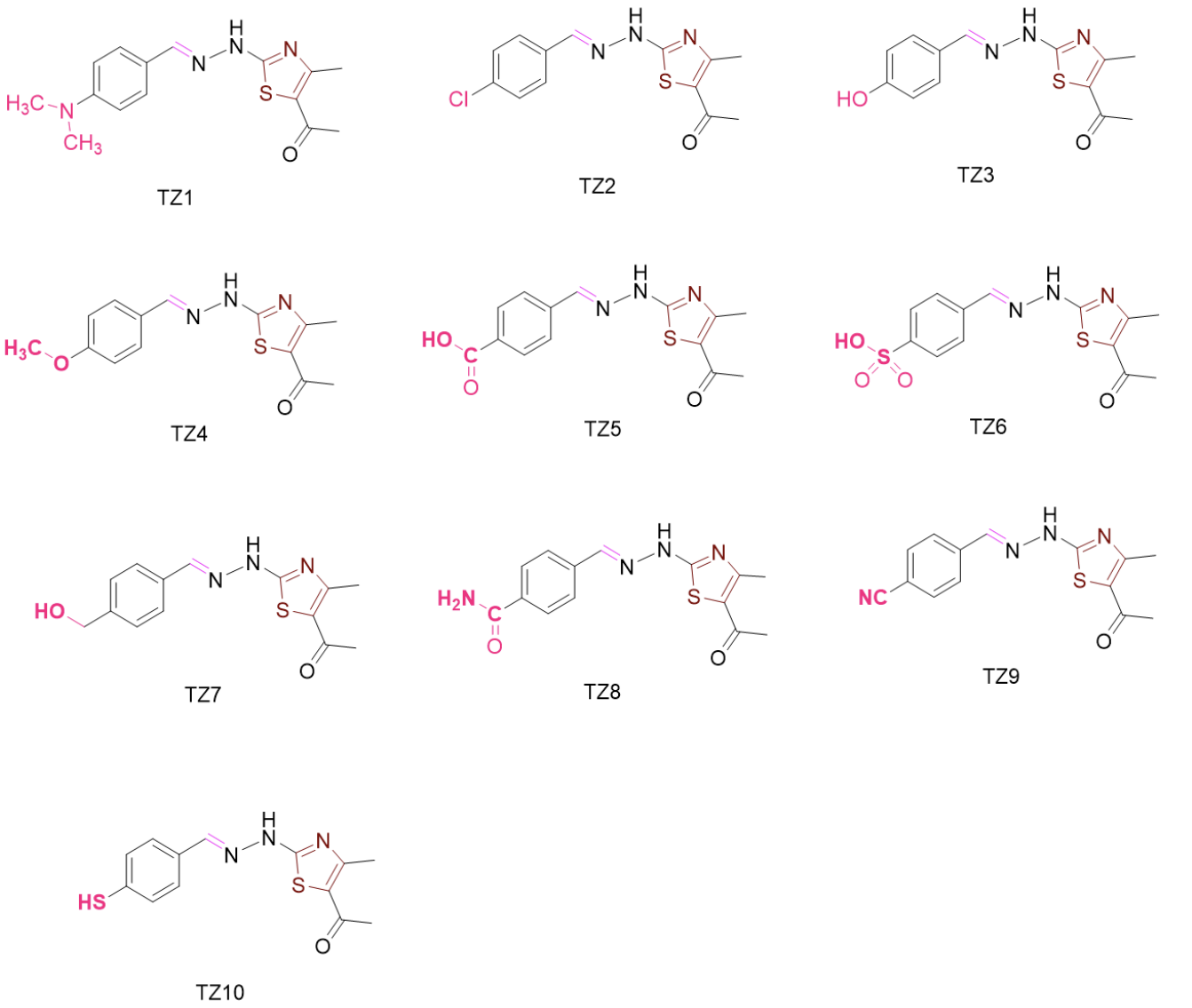

Figure 1. Designed new structures of thiazol derivatives

3.2. *In-silico* Study of Thiazole-Embedded Schiff Base Derivatives and Frontier Molecular Orbital Analysis

We designed ten Schiff base derivatives for further in-silico study, as illustrated in Figure 1. The optimized structures, shown in Figure S2, were calculated using Gaussian 09 W software, employing density functional theory (DFT) for optimization. Frontier molecular orbital (FMO) analysis was conducted to assess the Highest Occupied Molecular Orbital (HOMO) and the Lowest Unoccupied Molecular Orbital (LUMO), which play a crucial role in determining chemical reactivity. The HOMO reflects the ability of a molecule to donate electrons, while the LUMO indicates its capacity to accept electrons. The energy difference between these orbitals ($\Delta E = E_{LUMO} - E_{HOMO}$) is a key parameter for understanding the stability and reactivity of the compounds.

Table 1 presents the calculated values for E_{HOMO}, E_{LUMO}, and the energy gap (ΔE) for compounds TZ1-10. The HOMO energy values (E_{HOMO}) range from -0.17413 to -0.25362, indicating the highest occupied molecular orbitals. The LUMO energy values (E_{LUMO}) span from -0.05563 to -0.19278, representing the energy levels of the lowest unoccupied orbitals,

where more negative LUMO values suggest a greater ability to accept electrons. The HOMO-LUMO energy map is provided in Figure S1.

The HOMO-LUMO energy gap (ΔE) ranges from 0.02533 to 0.14029, with larger gaps indicating increased molecular stability. The hardness (η), representing the resistance to deformation of the electron cloud, shows negative values between 0.01267 and 0.07015. Softness (σ), which is inversely related to hardness, varies from 14.2572 to 78.9578, suggesting that compounds with higher softness may exhibit higher reactivity.

Electronegativity (μ) values range from -0.13966 to -0.2332, with more negative values indicating stronger electron-attracting tendencies. Chemical potential (χ) values, closely linked to electronegativity, vary from 0.11488 to 0.2232. Lastly, electronophilicity (ω) values, which are very low (0.111371 to 1.487589), suggest that these compounds have a limited tendency to accept electrons.

Table 1. Chemical reactivity of TZ1-10

TZs	E_{HOMO}	E_{LUMO}	ΔE	η	σ	μ	χ	ω
TZ1	-0.17413	-0.05563	0.1185	0.05925	16.8776	-0.11488	0.11488	0.111371
TZ2	-0.21524	-0.07496	0.14028	0.07014	14.2572	-0.1451	0.1451	0.150086
TZ3	-0.20127	-0.06098	0.14029	0.07015	14.2562	-0.13113	0.131125	0.122559
TZ4	-0.21783	-0.11970	0.09813	0.04907	20.3811	-0.16877	0.168765	0.290244
TZ5	-0.25362	-0.19278	0.06084	0.03042	32.8731	-0.2232	0.2232	0.81884
TZ6	-0.20678	-0.18145	0.02533	0.01267	78.9578	-0.19412	0.194115	1.487589
TZ7	-0.23287	-0.13715	0.09572	0.04786	20.8943	-0.18501	0.18501	0.357592
TZ8	-0.23464	-0.11653	0.11811	0.05906	16.9334	-0.17559	0.175585	0.261029
TZ9	-0.24895	-0.14713	0.10182	0.05091	19.6425	-0.19804	0.19804	0.385188
TZ10	-0.19957	-0.07974	0.11983	0.05992	16.6903	-0.13966	0.139655	0.16276

N.B.: global hardness (η), chemical potential (μ), softness (σ) electronegativity (χ), global electrophilicity index (ω).

3.3. Drug-likeness and Pharmacokinetic Characteristics

The molecular properties of TZ compounds, such as bioavailability and membrane permeability, are influenced by key factors like partition coefficient (logP), molecular weight (MW), and the number of hydrogen bond donors and acceptors, following Lipinski's "rule of five." As shown in Table 2, the molecular weight (MW) of these compounds ranges from 275.33 to 339.40 g/mol. Most of the TZ derivatives comply with Lipinski's rule, which applies to compounds with a molecular weight of less than 500 g/mol. The number of rotatable bonds ranges from four to six, where fewer rotatable bonds are often linked to improved bioavailability. The hydrogen bond properties show that most compounds have around six donors and one or two acceptors, both of which are crucial for solubility and receptor interactions. The Topological Polar Surface Area (TPSA) values range from 82.59 Å² to 145.34 Å², with lower TPSA (below 140 Å²) generally associated with better permeability and absorption, though TZ6 may have slightly reduced absorption. The consensus Log P values, indicating hydrophobicity, range from 1.71 to 3.30, with values between 1 and 3 typically showing optimal permeability and solubility.

Notably, TZ2 presents no Lipinski violations, shows low skin permeability (-5.29), has an excellent Log P (3.30), and a low molecular weight. TZ10 also stands out with no violations, an ideal Log P (2.99), and a low TPSA (121.39 Å²), while TZ9 exhibits good bioavailability due to its moderate Log P (2.54), acceptable molecular weight, and low TPSA.

Table 2. ADME properties of of TZ derivatives

TZ Derivatives	*MW (g/mol)*	*Num rotatable bonds*	*Num H bonds acceptors*	Num H bond donors	*TPSA (A2)*	*Consensus Log Po/w*	*Log Kp(skin permeation) cm/s*	*Lipinski rule*	*Violation*
TZ1	302.40	5	6	1	85.83	2.79	-5.70	Yes	0
TZ2	293.78	4	5	1	82.59	3.30	-5.29	Yes	0
TZ3	275.33	4	6	2	102.82	2.35	-5.87	Yes	0
TZ4	289.36	6	6	1	91.82	2.78	-5.73	Yes	0
TZ5	303.34	5	6	2	119.89	2.34	-6.13	Yes	0
TZ6	339.40	5	7	2	145.34	1.71	-6.90	Yes	0
TZ7	289.36	5	6	2	102.82	2.30	-6.34	Yes	0
TZ8	302.36	5	6	2	125.68	1.92	-6.58	Yes	0
TZ9	284.34	4	6	1	106.38	2.54	-5.88	Yes	0
TZ10	291.40	4	6	2	121.39	2.99	-5.61	Yes	0

Bioactivity score of TZ 1-10

The bioactivity scores of TZ compounds 1-10 were assessed. The drug-likeness of the lead compounds was evaluated using Molinspiration (https://www.molinspiration.com/cgi/properties), incorporating a range of factors, including GPCR modulators, ion channel modulators, kinase inhibitors, nuclear receptor ligands, protease inhibitors, and enzyme inhibitors (see Table 3). These combinations were analyzed to identify compounds suitable for further drug development. The bioactivity scores provide insights into the binding profiles of the compounds, which are useful in designing new drugs with improved selectivity and fewer side effects. Among the compounds, TZ6 displayed the fewest negative scores, suggesting higher overall bioactivity, particularly in its ability to bind GPCRs (-0.56) and inhibit enzymes (-0.28). TZ7 also demonstrated moderate activity, especially as a protease inhibitor (-1.08) and kinase inhibitor (-0.81).

Table 3. Bioactivity score of *TZ 1-10*

Drug	*GPCR ligand*	*Ion channel modulator*	*Kinase inhibitor*	*Nuclear receptor ligand*	*Protease inhibitor*	*Enzyme inhibitor*
TZ1	- 0.73	- 1.20	- 0.77	- 1.12	- 1.16	- 0.49
TZ2	- 0.90	- 1.29	- 1.00	- 1.38	- 1.39	- 0.58
TZ3	- 0.84	- 1.23	- 0.93	- 1.17	- 1.32	- 0.47
TZ4	- 0.86	- 1.31	- 0.93	- 1.25	- 1.29	- 0.56
TZ5	- 0.72	- 1.17	- 0.85	- 0.96	- 1.09	- 0.40
TZ6	- 0.56	- 1.02	- 0.88	- 1.34	- 0.81	- 0.28
TZ7	- 0.70	- 1.11	- 0.81	- 1.08	- 1.03	- 0.34
TZ8	- 0.72	- 1.25	- 0.67	- 1.27	- 1.03	- 0.43
TZ9	- 0.79	- 1.22	- 0.76	- 1.11	- 1.21	- 0.44
TZ10	- 0.96	- 1.47	- 1.14	- 1.53	- 1.25	- 0.49

3.4. Molecular Docking

3.4.1. *Protein selection*

Molecular docking is instrumental in drug discovery as it identifies potential therapeutic candidates, enhances the efficacy of existing medications, and elucidates the molecular basis of biological processes. This study selected proteins 4FX3, 4OAR, 3NUP, and 3ERT for their critical roles in hormone-dependent breast cancer and inflammation. Estrogen receptor alpha (4FX3) and aromatase (4OAR) are key in hormone signaling and cancer cell proliferation, making them vital for evaluating anti-cancer compounds. Nuclear Factor-kappa B (3NUP) regulates inflammation and cancer progression, while estrogen receptor beta (3ERT) is involved in apoptosis and hormone signaling. The thiazole-embedded Schiff base derivatives, particularly TZ6 and TZ8, demonstrated high binding affinities with these proteins, indicating potential as anti-cancer and anti-inflammatory agents. This targeted approach enhances the understanding of these compounds' therapeutic potential and guides further optimization for clinical applications. Table 5 shows that the TZ derivatives (TZ1-10) exhibit excellent docking performance, interacting with significant amino acids. Docking 55 complexes of four proteins with eleven TZ derivatives revealed specific protein targets related to the biological activity of the TZ drugs. TZ9 and TZ8 showed the highest affinities, indicating moderate interaction levels. Compounds like TZ2, TZ7, and TZ8 had strong interactions with the 3NUP receptor, highlighting its significance in the substance's mechanism of action. TZ9 and TZ8 also showed significant affinities, underscoring this receptor as crucial for the bioactivity of TZ drugs.

Table 4. Protein functions

PDB ID	Functions
4FX3	Phosphorylation of proteins involved in the G2, M transition by Cyclin A:Cdc2 complexes, cyclin A2-CDK1 complex, cell cycle G1/S phase transition, cellular response to cocaine, Transcription of E2F targets under negative control by p107 (RBL1) and p130 (RBL2) in complex with HDAC1
4OAR	glandular epithelial cell maturation, Loss of MECP2 binding ability to the NCoR/SMRT complex, negative regulation of androgen receptor signaling pathway, tertiary branching involved in mammary gland duct morphogenesis
3NUP	Multivesicular body, internal vesicle lumen, negative regulation of cardiocyte differentiation, positive regulation of protein kinase C activity, Shc-EGFR complex, epidermal growth factor receptor activity
3ERT	G protein-coupled estrogen receptor activity, regulation of epithelial cell apoptotic process, antral ovarian follicle growth, regulation of branching involved in prostate gland morphogenesis,

Table 5. Molecular Docking scores of selected TZ1-10 compounds with the four receptors.

Compound/Docking score (k/cal)	4FX3	4OAR	3NUP	3ERT
TZ1	-6.7	-7.3	-7.0	-6.6
TZ2	-7.8	-7.7	-7.6	-6.5
TZ3	-7.6	-7.6	-7.2	-6.8
TZ4	-7.4	-7.6	-6.6	-6.6
TZ5	-7.9	-7.4	-6.8	-7.6
TZ6	-8.0	-7.6	-6.8	-7.1
TZ7	-7.7	-7.6	-6.5	-7.1
TZ8	-8.2	-7.5	-7.0	-7.3
TZ9	-7.9	-7.8	-6.4	-7.4
TZ10	-7.2	-6.7	-6.3	-6.5

In Table 6, derivatives TZ8 and TZ6 demonstrated the highest binding affinities towards the 4FX3 receptor, with docking scores (S) of -8.2 and -8.0 kcal/mol, respectively. The derivative TZ8 formed three hydrogen bonds with LEU83 at distances of 1.95 Å, 2.25 Å, and 2.11 Å, and three hydrogen bonds with PHE82. Derivative TZ6 exhibited the formation of five hydrogen bonds involving LYS33, ASP86, LEU83, GLN85, with distances of 2.46 Å, 2.10 Å, 2.47 Å, 2.79 Å, and 2.83 Å, respectively. However, TZ5 and TZ9 displayed different interactions with 4FX3 despite having identical binding affinities. TZ5 established five hydrogen bonds with LEU83, LYS33, and GLN85, at distances of 2.35 Å, 2.67 Å, 2.16 Å, 2.73 Å, and 2.60 Å, respectively. TZ9 formed two hydrogen bonds with LEU83 and PHE82 at distances of 1.20 Å and 2.77 Å.

Table 6. Molecular Docking score of FDA approval drug

FDA approved drugs	4FX3	4OAR	3NUP	3ERT
Anastrozole	-8.1	-6.8	-8.2	-7.9
Doxorubicin	-8.5	-8.3	-8.4	-7.8
Gemcitabine	-7.6	-6.7	-6.6	-7.3
Tamoxifen	-5.7	-8.5	-6.2	-5.7

FDA-approved drugs generally exhibit stronger binding affinities, with Doxorubicin and Tamoxifen displaying the lowest energy values (-8.4 and -8.5 kcal/mol, respectively). Among the TZ compounds, TZ8 shows the strongest binding with the 4FX3 receptor (-8.2 kcal/mol), which is comparable to the binding strength of Doxorubicin. The binding affinities of FDA-approved medications range from -5.7 to -8.5 kcal/mol. Compared to these medications, the TZ compounds demonstrate slightly weaker binding strengths, ranging from -6.3 to -8.2 kcal/mol. FDA-approved medications generally exhibit greater and more consistent binding across receptors compared to the TZ1-10 compounds. This suggests that while FDA-approved medications may be more efficient, the TZ compounds—notably TZ8—still show competitive binding, particularly with 4FX3. These findings indicate the potential for further optimization of TZ compounds to enhance their binding affinities to levels comparable to or exceeding those of FDA-approved medications.

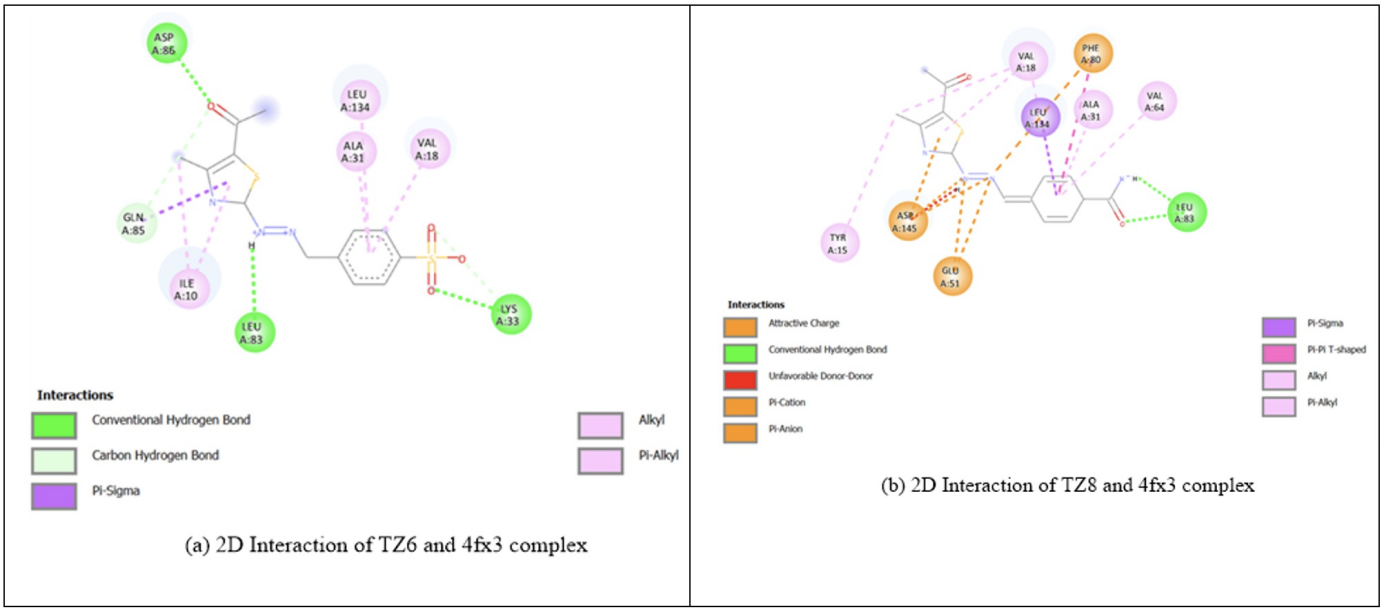

Figure 2. (a) 2D Interection of TZ6 + 4fx3 complex. (b) 2D Interection of TZ8 + 4fx3 complex.

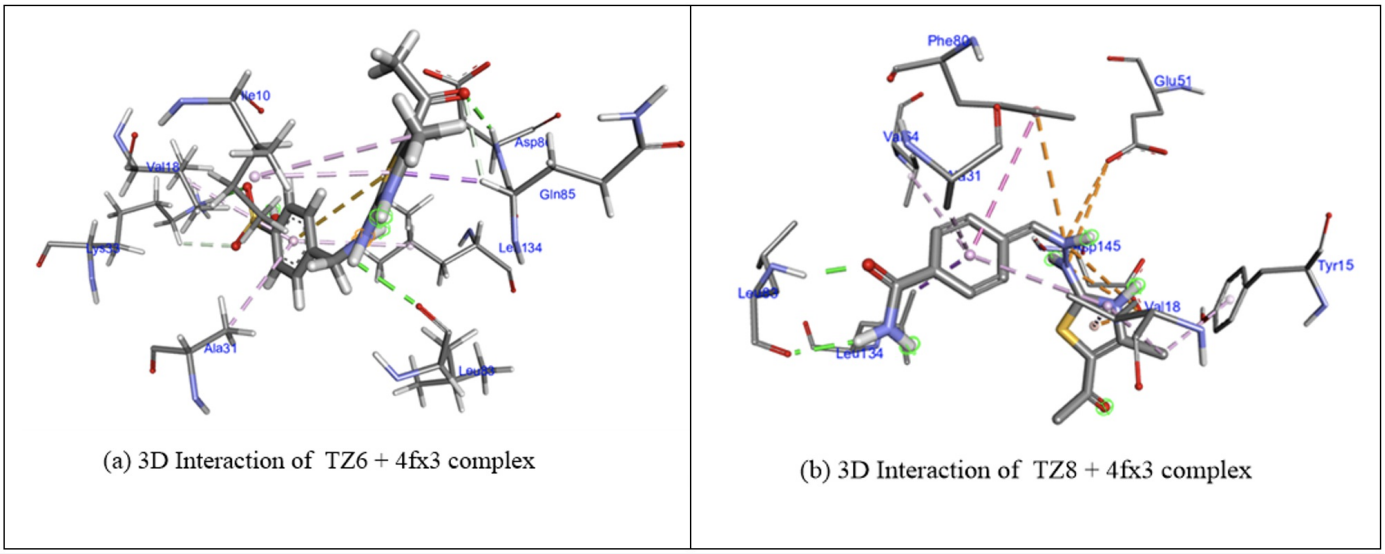

Figure 3. (a) 3D Interection of TZ6 + 4FX3 complex. (b) 3D Interection of TZ8 + 4FX3 complex.

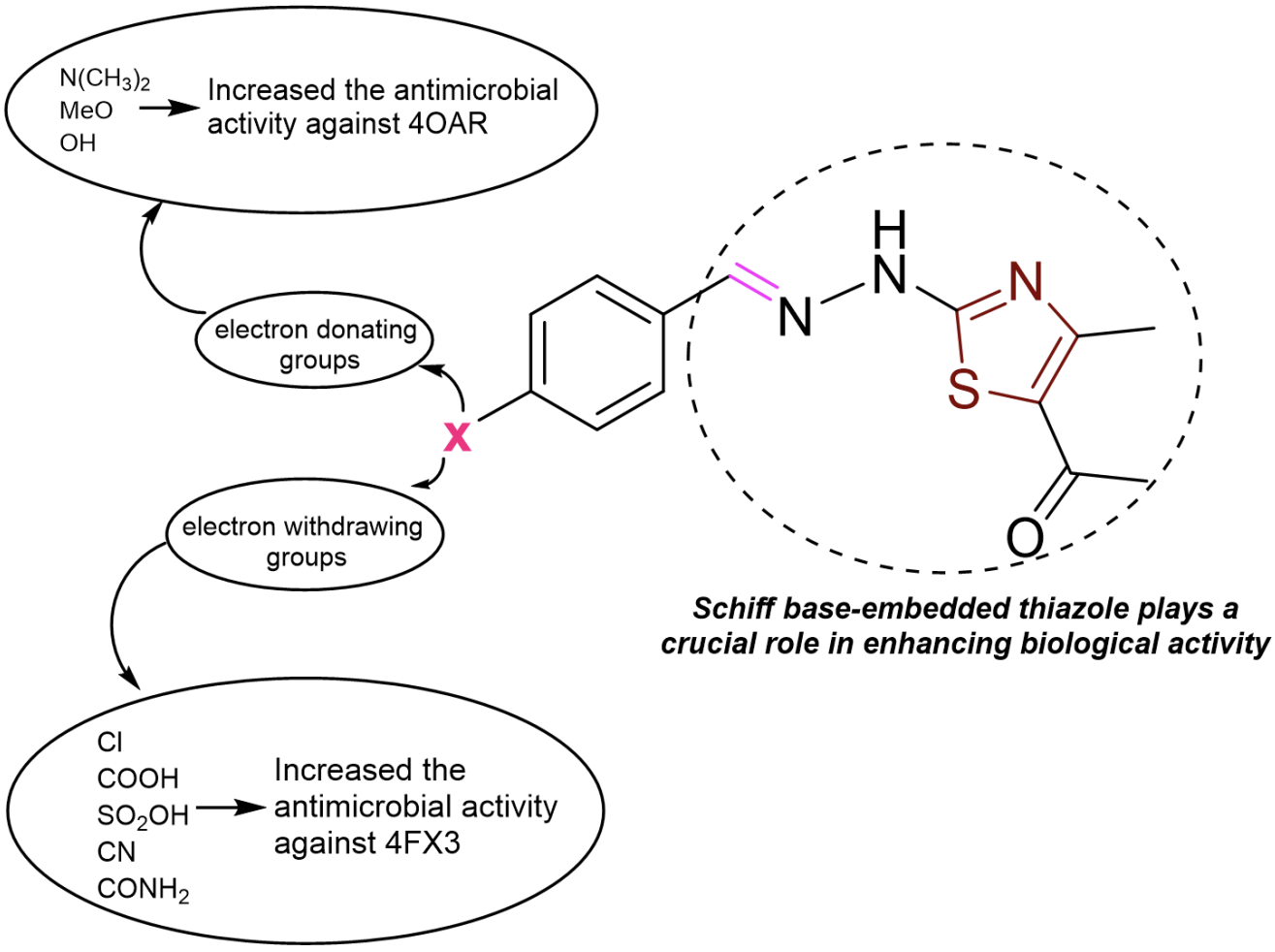

Figure 4. Structure activity relationship study of the TZ derivatives.

Figure 4 illustrates the crucial role of electron-donating and electron-withdrawing groups in modulating the antibacterial activity of a thiazole-based compound. The figure demonstrates the impact of substituents on the antibacterial properties

of the compound, highlighting the significance of these groups in controlling biological activity. At the core of the figure is a thiazole ring structure, renowned for its biological relevance in numerous medicinal compounds. The basic structure being studied consists of an aryl group and an acetyl group attached to the thiazole ring. The letter "X" marks a position on the aryl ring where various substituents can be introduced, significantly altering the compound's antibacterial action.

The figure 4 reveals that antimicrobial activity against the 4OAR strain is enhanced by the introduction of electron-donating groups such as dimethylamino ($N(CH_3)_2$), methoxy (MeO), and hydroxy (OH) at the X position. These groups increase the electron density of the ring, potentially improving the compound's efficacy by strengthening its interaction with microbial enzymes or cell membranes. Conversely, electron-withdrawing groups like cyano (CN), amide ($CONH_2$), sulfonic acid (SO_2OH), carboxylic acid (COOH), and chloride (Cl) enhance antibacterial activity against the 4FX3 strain. These groups decrease the electron density of the ring, which may heighten the molecule's binding affinity to microbial targets and boost its antibacterial activity.

Moreover, the figure clearly shows that modifying the substituents at the X position can fine-tune the antibacterial activity of the thiazole-based molecule. The distinct roles of electron-donating and electron-withdrawing groups in targeting different bacterial strains provide a strategic approach to developing more effective antimicrobial drugs.

4. Conclusion

This study highlights the synthesis and in-silico evaluation of ten novel thiazole-embedded Schiff base derivatives (TZ1-10) in comparison with four FDA-approved breast cancer treatments. Notably, TZ6 and TZ8 exhibited superior oral bioavailability and promising ADME profiles, along with significant docking scores surpassing -6 kcal/mol. These compounds demonstrated strong binding affinities, particularly towards the 4FX3 protein, and presented low toxicity with no carcinogenic properties. The insights garnered from this research suggest that TZ6 and TZ8 hold considerable potential as anticancer agents. Future work will focus on optimizing the molecular structure of these compounds to enhance their binding affinities further and improve their therapeutic efficacy. Additionally, in-vitro and in-vivo studies are necessary to confirm these computational predictions and assess the full pharmacological potential of these derivatives. These efforts could ultimately contribute to the development of new, more effective, and targeted treatments for breast cancer, offering an alternative to current therapies that often suffer from resistance and adverse side effects.

Statements and Declarations

Conflict of Interests

The authors declare no competing financial interest.

Acknowledgments

We are grateful to the Chittagong University of Engineering and Technology (CUET), Chattogram, Bangladesh for all kinds of experimental and financial supports.

References

1. ^*Hameed A, Al-Rashida M, Uroos M, Abid Ali S, Khan KM. Schiff bases in medicinal chemistry: a patent review (2010-2015). Expert opinion on therapeutic patents 2017; 27(1): 63-79.*
2. ^*Bharti S, Nath G, Tilak R, Singh S. Synthesis, anti-bacterial and anti-fungal activities of some novel Schiff bases containing 2, 4-disubstituted thiazole ring. European journal of medicinal chemistry 2010; 45(2): 651-660.*
3. ^*Mushtaq I, Ahmad M, Saleem M, Ahmed A. Pharmaceutical significance of Schiff bases: An overview. Future Journal of Pharmaceutical Sciences 2024; 10(1): 16.*
4. ^*Kostova I, Saso L. Advances in research of Schiff-base metal complexes as potent antioxidants. Current medicinal chemistry 2013; 20(36): 4609-4632.*
5. ^*Pisanu F, Sykula A, Sciortino G, Maseras F, Lodyga-Chruscinska E, Garribba E. Experimental and Computational Studies on the Interaction of DNA with Hesperetin Schiff Base CuII Complexes. International journal of molecular sciences 2024; 25(10): 5283.*
6. ^*Arshad MF, Alam A, Alshammari AA, Alhazza MB, Alzimam IM, Alam MA, Mustafa G, Ansari MS, Alotaibi AM, Alotaibi AA. Thiazole: A versatile standalone moiety contributing to the development of various drugs and biologically active agents. Molecules 2022; 27(13): 3994.*
7. ^*Petrou A, Fesatidou M, Geronikaki A. Thiazole ring—A biologically active scaffold. Molecules 2021; 26(11): 3166.*
8. ^*Feng Y, Spezia M, Huang S, Yuan C, Zeng Z, Zhang L, Ji X, Liu W, Huang B, Luo W. Breast cancer development and progression: Risk factors, cancer stem cells, signaling pathways, genomics, and molecular pathogenesis. Genes & diseases 2018; 5(2): 77-106.*
9. ^*Choi JE, Kim Z, Park CS, Park EH, Lee SB, Lee SK, Choi YJ, Han J, Jung KW, Kim HJ. Breast cancer statistics in Korea, 2019. Journal of Breast Cancer 2023; 26(3): 207.*
10. ^*Esteva FJ, Hubbard-Lucey VM, Tang J, Pusztai L. Immunotherapy and targeted therapy combinations in metastatic breast cancer. The lancet oncology 2019; 20(3): e175-e186.*
11. ^*Xia Y, Sun M, Huang H, Jin WL. Drug repurposing for cancer therapy. Signal Transduction and Targeted Therapy 2024; 9(1): 92.*
12. ^*Al-Amiery A, Isahak WNRW, Al-Azzawi WK. Multi-method evaluation of a 2-(1, 3, 4-thiadiazole-2-yl) pyrrolidine corrosion inhibitor for mild steel in HCl: combining gravimetric, electrochemical, and DFT approaches. Scientific Reports 2023; 13(1): 9770.*
13. a, b*Caricato M, Frisch MJ, Hiscocks J, Frisch MJ. Gaussian 09: IOps Reference; Gaussian Wallingford, CT, USA, 2009.*
14. ^*Nath A, Kumer A, Khan MW. Synthesis, computational and molecular docking study of some 2, 3-dihydrobenzofuran and its derivatives. Journal of Molecular Structure 2021; 1224: 129225.*

15. ^*Li C, Xie Y, Hu S, Yu H, Xu Y, Shen H, Yuan Y, Gu L, Pu B. Identification of formononetin as the active compound of CR-SR in hepatocellular carcinoma treatment: An integrated approach combining network pharmacology and weighted gene co-expression networks. Chemical Biology & Drug Design 2024; 103(1): e14363.*

16. ^*Kitete Mulongo E, Kilembe Thambwe J, Matondo A, Ngbolua KT-N, Tshilanda D, Mungu Yvette N-U, Tshibangu D, Tshimankinda Mpiana P. The Potential of Compounds Derived from Jatropha Curcas Against Pr and Herα in Breast Cancer Treatment: Molecular Docking and Molecular Dynamics Simulation Studies.*

17. ^*Jiang C, Ye Y, Kang W, Yang J, He Z, Cao Q, Lian C, Xing Y, Yang Q, Zhao J. Elucidating Binding Selectivity in Cyclin-Dependent Kinases (CDKs) 4, 6, and 9: Development of Highly Potent and Selective CDK4/9 Inhibitors. 2024.*

18. ^*Somturk-Yilmaz B, Turkmenoglu B, Akkoc SS. Synthesis, Characterization, Cytotoxic Activity Studies of N1-phenylbenzene-1, 2-diamine@ CuhNFs and 1, 2-phenylenediamine@ CuhNFs, and Molecular Docking Calculations of Their Ligands. Journal of Inorganic and Organometallic Polymers and Materials 2024; 1-13.*

19. ^*Trott O, Olson AJ. AutoDock Vina: improving the speed and accuracy of docking with a new scoring function, efficient optimization, and multithreading. Journal of computational chemistry 2010; 31(2): 455-461.*

20. ^*Dallakyan S, Olson AJ. Small-molecule library screening by docking with PyRx. Chemical biology: methods and protocols 2015; 243-250.*

21. [a, b]*Jejurikar BL, Rohane SH. Drug designing in discovery studio. 2021.*

22. ^*Suganya M, Jose Kavitha S, Raja Kannan V. Insilco Studies of Molecular Property and Bioactivity of Organic Crystalline Compounds using Molinspiration. International Research Journal of Engineering and Technology 2020.*